Passive Suppression of Nonlinear Panel Flutter Using Piezoelectric Materials with Resonant Circuit

Seong Hwan Moon
Department of Aerospace Engineering, Seoul National University, San 56-1, Shinrim-Dong, Kwanak-Gu, Seoul 151-742, Korea
Chul Yong Yun
Department of Aerospace Engineering, Seoul National University, San 56-1, Shinrim-Dong, Kwanak-Gu, Seoul 151-742, Korea
Seung Jo Kim*
Department of Aerospace Engineering, Seoul National University, San 56-1, Shinrim-Dong, Kwanak-Gu, Seoul 151-742, Korea

In this study, a passive suppression scheme for nonlinear flutter problem of composite panel, which is believed to be more reliable than the active control methods in practical operations, is proposed. This scheme utilizes a piezoelectric inductor-resistor series shunt circuit. The finite element equations of motion for an electromechanically coupled system is derived by applying the Hamilton's principle. The aerodynamic theory adopted for the present study is based on the quasi-steady piston theory, and von-Karman nonlinear strain-displacement relation is also applied. The passive suppression results for nonlinear panel flutter are obtained in the time domain using the Newmark-β method. To achieve the best damping effect, optimal shape and location of the piezoceramic(PZT) patches are determined by using genetic algorithms. The effects of passive suppression are investigated by employing in turn one shunt circuit and two independent shunt circuits. Feasibility studies show that two independent inductor-resistor shunt circuits suppresses flutter more effectively than a single shunt circuit. The results clearly demonstrate that the passive damping scheme that uses piezoelectric shunt circuit can effectively attenuate the flutter.

Key Words: Nonlinear Panel Flutter, Passive Suppression, PZT

Nomenclature

a	: Panel length
b	: Panel width
$\mathbf{c}$	: Elastic stiffness matrix
d_{31}	: Piezoelectric constant(strain/charge)
D_3	: Electrical displacement (charge/area in the z direction)
h	: Panel thickness
$\mathbf{h}$	: Piezoelectric constant matrix
L	: Inductance
p_a	: Freestream aerodynamic pressure
Q	: Charge
R	: Resistance
u, v, w	: Displacements
V_3	: Applied voltage
V_{3max}	: Maximum applied voltage
V_∞	: Freestream velocity
$\Delta T(x,y,z)$	: Temperature change
α	: Thermal expansion coefficient
$\boldsymbol{\varepsilon}, \{\varepsilon\}$	: Strain vectors
$\boldsymbol{k}, \{k\}$	: Curvature vector
λ	: Nondimensional aerodynamic pressure

* Corresponding Author,
E-mail : sjkim@snu.ac.kr
TEL : +82-2-880-7388; **FAX** : +82-2-887-2662
Department of Aerospace Engineering, Seoul National University, San 56-1, Shinrim-Dong, Kwanak-Gu, Seoul 151-742, Korea (Manuscript **Received** November 30, 2000; **Revised** October 12, 2001)

σ,$\{\sigma\}$: Stress vectors
τ : Nondimensional time($\omega_0 t$)
Φ : Normal mode vector

Superscripts

D : At constant electric displacement
S : At constant strain
t : At constant stress
T : Transpose

Subscripts

a : Air
b : Bending
h : Host structure(composite plate)
m : Membrane
p : Piezoelectric material

1. Introduction

The panel flutter is a self-excited aeroelastic phenomenon. It is caused and maintained by the interactions between the motions of an aircraft structural panel and the aerodynamic load exerted on that panel. It occurs most frequently in supersonic/hypersonic flows, and the inclusion of a thermal effect by aerodynamic heating tends to reduce the panel stiffness (thermally induced geometry stiffness decreases when the thermal load increases), which enables flutter motion to occur at lower dynamic pressures than in the absence of the thermal influence.

The linear analysis of the panel flutter can predict airflow speed at which the panel becomes dynamically unstable and the amplitude of oscillation starts to grow exponentially with time. In reality, the nonlinear effect of the panel starts to appear after the amplitude has increased to a certain level, and the vibration level reaches a bounded value (so-called limit-cycle)

During the past few years, a significant amount of research has been reported in the field of control of flexible structures by the use of piezoelectric materials (Nam and Kim, 1996 ; Lee et al., 1999).

Many works on the suppression of nonlinear panel flutter by using the piezoelectric material or shape memory alloy have been carried out. Scott and Weissharr (1994) performed an active suppression research on increasing the flutter velocity by using the piezoceramic and shape memory alloys based on the linear plate theory and Ritz method. Zhou *et al* (1995) used the finite element method to suppress the nonlinear panel flutter under a uniform thermal loading by applying a modal reduction scheme and LQR linear control. The feasibility of passively dissipating mechanical energy with electrical shunt circuits was investigated. Hagood and von Flotow (1991) formulated the equations of the mechanical and electrical motion with piezoelectric material shunted with electrical circuits composed of a resistor alone or an inductor-resistor resonant shunt to provide damping for the beam. Hollkamp (1994) showed that multiple modes could be suppressed by using a single piezoelectric patch connected to multiple inductor-resistor-capacitor for a beam model. Tang *et al.* (1999) showed that the structural vibration could be suppressed effectively by using the active-passive hybrid piezoelectric network for a beam model. However, most of the previous papers on resonant-shunted piezoelectrics have a serious limitation in that the theories are applied to the case of the uniaxial loading on the beam. For more complex structures and loading conditions, the aforementioned works need to be modified to give reasonable solutions. Hollkamp and Gordon (1995) investigated a suppression scheme for two-dimensional planar problems by using a passive piezoelectric network. Lag mode suppression of hingeless helicopter rotor blade was investigated by Kim *et al.* (1999) using the passive piezoelectric damping scheme.

Previous studies on suppression of the nonlinear panel flutter have been carried out by applying active control methods. However, application of the active control methods to practical flutter problems have major disadvantages in that a large amount of power is required to operate actuators, and additional hardware such as sensors and controllers is needed. In this paper, an efficient piezoelectric passive damper is devised for suppressing the nonlinear panel flutter by applying the finite element method. For effective damping, a genetic algorithm (Goldberg,

1989) was devised to obtain the optimal shape and locations of the piezoceramic material(PZT) that maximizes the modal damping force for the controlled modes. For a shunted model, there are two kinds of piezoelectric shunt circuits: one is composed of a resistor alone and the other is a combination of a resistor and an inductor. Here we focus on the electric circuit that consists of inductor(L)-resistor(R) elements in series, where the device creates an electrical resonance by properly tuning the shunt circuit and also increases the damping of the system. Its behavior is analogous to that of a mechanical vibration absorber. In this study, a single piezoelectric shunt circuit and two independent shunt circuits are used in turn for suppression of the nonlinear panel flutter. Optimal resistance and inductance values are determined by the pole placement method. The governing equations of the panel, connected to an electric circuit consisting of a resistor and an inductor in series, are derived from the Hamilton's principle taking into account the von Karman plate theory and the thermal effect by aerodynamic heating. The aerodynamic force applied is based on the quasi-steady first-order piston theory. The equations of motion of the piezoelectrics and shunted circuit as well as the plate are discretized by the finite element method. The modal reduction is carried out with the first few modes in airflow direction and only the first mode in the spanwise direction. Using the Newmark-β method, results of the passive suppression for a simply supported composite panel are presented in the time domain.

2. Constitutive Equations

The linear piezoelectric constitutive equations of a piezoelectric material can be written as follows:

$$\begin{aligned}\boldsymbol{\sigma}&=\boldsymbol{c}^D\boldsymbol{\varepsilon}-\boldsymbol{h}^T\boldsymbol{D}\\ \boldsymbol{E}&=-\boldsymbol{h}\boldsymbol{\varepsilon}+\boldsymbol{\beta}^S\boldsymbol{D}\end{aligned}\tag{1}$$

where $\boldsymbol{\sigma}$ and $\boldsymbol{\varepsilon}$ represent the mechanical stresses and engineering strains in vectorial notations, respectively. $\mathbf{E}$ is the electric field vector (volts/length along the transverse direction), and $\mathbf{D}$ is the electric displacement vector(charge/area in the transverse direction). $\mathbf{c}$ represents the elastic stiffness matrix of piezoelectric material, and superscripts $(\,)^S$ and $(\,)^D$ denote that the values are measured at constant strain field and electric displacement field, respectively. The superscript $(\,)^T$ denotes transposition of a matrix.

For a piezoelectric material polarized in the thickness direction("3" direction), impermittivity components $\boldsymbol{\beta}^S$ are expressed as follows:

$$\boldsymbol{\beta}^S=\begin{bmatrix}1/\in_{11}^S & 0 & 0\\ 0 & 1/\in_{11}^S & 0\\ 0 & 0 & 1/\in_{33}^S\end{bmatrix}\tag{2}$$

and piezoelectric coefficient $\mathbf{h}$ can be expressed as follows:

$$\mathbf{h}=\begin{bmatrix}0 & 0 & 0 & 0 & h_{15} & 0\\ 0 & 0 & 0 & h_{15} & 0 & 0\\ h_{31} & h_{31} & h_{33} & 0 & 0 & 0\end{bmatrix}\tag{3}$$

where $\in$ is the dielectric constant and the material is approximately isotropic in the "1" and "2" directions.

For a piezoelectric material under plane stress, the piezoelectric coefficient matrix $\mathbf{h}$ can be expressed as follows:

$$\mathbf{h}=[h_{31}\;\; h_{31}\;\; 0]\tag{4}$$

where the piezoelectric constant h_{31} can be written as [see Appendix]

$$h_{31}=g_{31}(c_{11}^D+c_{12}^D)=\frac{d_{31}E^D}{\in_{33}^t(1-\nu)}\tag{5}$$

and superscript $(\,)^t$ denotes that the values are measured at constant stress.

Then, the stress-strain relationships of the isotropic piezoelectric layer subjected to a temperature variation $\Delta T(x,\ y,\ z)$ due to aerodynamic heating in the supersonic flow is expressed as follows:

$$\begin{Bmatrix}\sigma_x\\ \sigma_y\\ \tau_{xy}\end{Bmatrix}_p=\left(\frac{E^D}{1-\nu^2}\right)_p\begin{bmatrix}1 & \nu & 0\\ \nu & 1 & 0\\ 0 & 0 & (1-\nu)/2\end{bmatrix}_p\begin{Bmatrix}\varepsilon_x\\ \varepsilon_y\\ \gamma_{xy}\end{Bmatrix}-\left(\frac{E^D\alpha}{1-\nu}\right)_p\begin{Bmatrix}\Delta T\\ \Delta T\\ 0\end{Bmatrix}-D_3\begin{Bmatrix}h_{31}\\ h_{31}\\ 0\end{Bmatrix}_p\tag{6}$$

and the electric field becomes

$$E_3=\frac{1}{\in_{33}^S}D_3-[h_{31}\ h_{31}\ 0]\begin{Bmatrix}\varepsilon_x\\ \varepsilon_y\\ \gamma_{xy}\end{Bmatrix} \tag{7}$$

where subscript p represents piezoelectric material.

For k-th layer of a composite plate, the constitutive equations based on the plane stress state can be written as follows:

$$\begin{Bmatrix}\sigma_x\\ \sigma_y\\ \tau_{xy}\end{Bmatrix}_h^k=\begin{bmatrix}\bar{Q}_{11} & \bar{Q}_{12} & \bar{Q}_{16}\\ \bar{Q}_{12} & \bar{Q}_{22} & \bar{Q}_{26}\\ \bar{Q}_{16} & \bar{Q}_{26} & \bar{Q}_{66}\end{bmatrix}_h^k\left\{\begin{Bmatrix}\varepsilon_x\\ \varepsilon_y\\ \gamma_{xy}\end{Bmatrix}-\Delta T\begin{Bmatrix}\alpha_x\\ \alpha_y\\ \alpha_{xy}\end{Bmatrix}_h^k\right\} \tag{8}$$

where subscript h represents the host structure, α represents the thermal expansion coefficient, and $\bar{Q}_{ij}$ matrix denotes the transformed reduced stiffness.

The dynamic equilibrium equation of the composite plate integrated with the piezoelectric actuator is derived based on the classical laminated plate theory (CLPT). According to the Kirchhoff hypothesis, the displacement field (u, v, w) is expressed as

$$\begin{aligned}u(x,\ y,\ z,\ t)&=u_0(x,\ y,\ t)-z\frac{\partial w}{\partial x}\\ v(x,\ y,\ z,\ t)&=v_0(x,\ y,\ t)-z\frac{\partial w}{\partial y}\\ w(x,\ y,\ z,\ t)&=w_0(x,\ y,\ t)\end{aligned} \tag{9}$$

where (u_0, v_0, w_0) are the displacement field of a point on the mid-plane of the laminate. A laminate coordinate system is assumed such that x and y are the in-plane axes and the z-direction coincides with the thickness direction of the laminate.

By invoking von Karman's large deflection, we have the following Green-Lagrangian strain-displacement relations (Chia, 1980):

$$\begin{aligned}\boldsymbol{\varepsilon}&=\begin{Bmatrix}\varepsilon_x\\ \varepsilon_y\\ \gamma_{xy}\end{Bmatrix}=\begin{Bmatrix}u_{o,x}\\ v_{o,y}\\ u_{o,y}+v_{o,v}\end{Bmatrix}+\frac{1}{2}\begin{Bmatrix}w^2{}_{,x}\\ w^2{}_{,y}\\ 2w_{,x}w_{,y}\end{Bmatrix}\\ &-z\begin{Bmatrix}w_{,xx}\\ w_{,yy}\\ 2w_{,xy}\end{Bmatrix}=\boldsymbol{\varepsilon}_m+\boldsymbol{\varepsilon}_\theta+z\mathbf{k}\end{aligned} \tag{10}$$

where $(\ )_{,i}$ represents the partial derivative of $(\ )$ with respect to ith coordinate and $\boldsymbol{\varepsilon}_m$ is the linear membrane strain vector, $\boldsymbol{\varepsilon}_\theta$ is the nonlinear membrane strain vector due to large deflections, and $\mathbf{k}$ is the bending curvature vector.

3. Aerodynamic Theory

The transverse forces acting on the panel under a sufficiently high supersonic Mach number ($M>1.7$) flow can be suitably described by the quasi-steady first-order piston theory (Lee et al., 1999) given by

$$\begin{aligned}p_a&=-\frac{\rho_a V_\infty^2}{\beta}\left\{\cos\phi\frac{\partial w}{\partial x}+\sin\phi\frac{\partial w}{\partial y}\right.\\ &\left.+\left(\frac{M_\infty^2-2}{M_\infty^2-1}\right)\frac{1}{V_\infty}\frac{\partial w}{\partial t}\right\}\\ &=-\left(\lambda\frac{D}{a^3}\cos\phi\frac{\partial w}{\partial x}+\lambda\frac{D}{a^3}\sin\phi\frac{\partial w}{\partial y}\right.\\ &\left.+\frac{g_a\ D}{\omega_o\ a^4}\frac{\partial w}{\partial t}\right)\end{aligned} \tag{11}$$

where p_a is the freestream aerodynamic pressure and ρ_a is the air mass density. V_∞ is the freestream velocity, parameter β is defined by $\beta=(M_\infty^2-1)^{1/2}$, M_∞ is the Mach number, ϕ is the angle between the airflow and panel's x-axis, and a is the panel length. D is the first entry of the laminate bending stiffness matrix calculated when all the fibers of the composite layers are aligned in the direction of the airflow.

The nondimensional aerodynamic pressure parameter λ and nondimensional aerodynamic damping g_a can be expressed as follows:

$$\lambda=\rho_\infty V_\infty^2 a^3/\beta D,\ g_a=\frac{\rho_a V_\infty(M_\infty^2-2)}{\rho h\omega_o\beta^3} \tag{12}$$

where ρ is the mass density of the panel, and h is the panel thickness.

A convenient reference frequency is defined by

$$\omega_o=\sqrt{\frac{D}{\rho h a^4}} \tag{13}$$

Non-dimensional mass parameters such as air-panel mass ratio and the aerodynamic damping coefficient are introduced below:

$$\mu=\frac{\rho_a a}{\rho h},\ c_a=\left(\frac{M_\infty^2-2}{M_\infty^2-1}\right)\frac{\mu}{\beta} \tag{14}$$

For Mach number $M_\infty\gg1$,

$$g_a=\sqrt{(\lambda c_a)}\ \text{and}\ c_a=\mu/M_\infty \tag{15}$$

4. Governing Equations

For an electromechanically coupled system, equations of motion can be derived using the Hamilton's principle.

$$\delta\Pi=\delta\int_{t_1}^{t_2}(T-U)\,dt+\int_{t_1}^{t_2}\delta W dt=0 \quad (16)$$

$$T=\frac{1}{2}\int_V \rho(\dot{u}^2+\dot{v}^2+\dot{w}^2)\,dV \quad (17)$$

$$U=\frac{1}{2}\int_{V_h}\varepsilon^T\sigma_h dV+\frac{1}{2}\int_{V_p}\varepsilon^T\sigma_p dV+\frac{1}{2}\int_{V_p}D_3E_3dV \quad (18)$$

where T denotes the kinetic energy of the integrated system and U is the potential energy which consists of the strain energy and electrical energy. The virtual work due to the aerodynamic pressure and electric potential is qiven by

$$\delta W=(-L\ddot{Q}-R\dot{Q})\,\delta Q+\int_A \delta w^T p_a dA \quad (19)$$

where L and R are inductance and resistance in the shunt circuit, respectively. Q is the charge of piezoelectric material due to deformation.

Then, the potential energy is given by:

$$\begin{aligned}\delta U=\int_V[&\delta\varepsilon_m^T\bar{\mathbf{Q}}\varepsilon_m+\delta\varepsilon_m^T\bar{\mathbf{Q}}\varepsilon_\theta+\delta\varepsilon_m^T\bar{\mathbf{Q}}z\mathbf{k}\\&+\delta\varepsilon_\theta^T\bar{\mathbf{Q}}\varepsilon_m+\delta\varepsilon_\theta^T\bar{\mathbf{Q}}\varepsilon_\theta+\delta\varepsilon_\theta^T\bar{\mathbf{Q}}z\mathbf{k}\\&+z\delta\mathbf{k}^T\bar{\mathbf{Q}}\varepsilon_m+z\delta\mathbf{k}^T\bar{\mathbf{Q}}\varepsilon_\theta+z\delta\mathbf{k}^T\bar{\mathbf{Q}}z\mathbf{k}\\&+\delta\varepsilon_m^T\bar{\mathbf{Q}}\Delta T\alpha-\delta\varepsilon_\theta^T\Delta T\bar{\mathbf{Q}}\alpha\\&-z\delta\mathbf{k}^T\Delta T\bar{\mathbf{Q}}\alpha-\delta\varepsilon_m^T\mathbf{h}^TD_3-\delta\varepsilon_\theta^T\mathbf{h}^TD_3\\&-z\delta\mathbf{k}^T\mathbf{h}^TD_3+\delta D_3^T\frac{1}{\in_{33}^S}D_3\\&-\delta D_3^Th_{31}\varepsilon_x-\delta D_3^Th_{31}\varepsilon_y]dV\end{aligned} \quad (20)$$

In Eq. (20), the terms denoted by bars are derived from the electrical energy.

A 4-node conforming plate element is employed in this study. There are two in-plane degrees of freedom $(u,\ v)$ and four bending degrees of freedom $(w,\ w_{,x},\ w_{,y},\ w_{,xy})$ at each node.

$$\begin{aligned}\mathbf{w}_b^e=\{&w_1,\ w_{1x},\ w_{1y},\ w_{1xy},\ w_2,\ w_{2x},\ w_{2y},\ w_{2xy},\ w_3,\\&w_{3x},\ w_{3y},\ w_{3xy},\ w_4,\ w_{4x},\ w_{4y},\ w_{4xy}\}^T\\\mathbf{w}_m^e=\{&u_1,\ v_1,u_2,\ v_2,u_3,\ v_3,u_4,\ v_4\}^T\end{aligned} \quad (21)$$

The Lagrange and Hermite polynomials are used to interpolate each of the in-plane and bending displacements, respectively. The displacements $(u,\ v,\ w)$ can be expressed by nodal degrees of freedom as follows:

$$\begin{Bmatrix}u\\v\end{Bmatrix}=\begin{Bmatrix}\mathbf{N}_{mx}\\\mathbf{N}_{my}\end{Bmatrix}\mathbf{w}_m^e=\mathbf{N}_m\mathbf{w}_m^e,\quad w=\mathbf{N}_b\mathbf{w}_b^e \quad (22)$$

The membrane strain components and curvature can be expressed in terms of the nodal degrees of freedom

$$\varepsilon_m=\begin{Bmatrix}\mathbf{B}_{mx}\\\mathbf{B}_{my}\\\mathbf{B}_{mxy}\end{Bmatrix}\mathbf{w}_m^e=\mathbf{B}_m\mathbf{w}_m^e$$

$$\varepsilon_\theta=\frac{1}{2}\begin{Bmatrix}\left(\frac{\partial w}{\partial x}\right)^2\\\left(\frac{\partial w}{\partial y}\right)^2\\2\frac{\partial w}{\partial x}\frac{\partial w}{\partial y}\end{Bmatrix}=\frac{1}{2}\begin{Bmatrix}\left(\frac{\partial \mathbf{N}_b}{\partial x}\mathbf{w}_b{}^e\right)^2\\\left(\frac{\partial \mathbf{N}_b}{\partial y}\mathbf{w}_b{}^e\right)^2\\2\frac{\partial \mathbf{N}_b}{\partial x}\mathbf{w}_b^e\frac{\partial \mathbf{N}_b}{\partial y}\mathbf{w}_b^e\end{Bmatrix}$$

$$=\frac{1}{2}\begin{Bmatrix}(\mathbf{B}_{\theta x}\mathbf{w}_b^e)^2\\(\mathbf{B}_{\theta y}\mathbf{w}_b^e)^2\\2\mathbf{B}_{\theta x}\mathbf{w}_b^e\mathbf{B}_{\theta y}\mathbf{w}_b^e\end{Bmatrix}=\frac{1}{2}\begin{Bmatrix}\mathbf{w}_b^{e\,T}\mathbf{B}_{\theta x}^T\mathbf{B}_{\theta x}\mathbf{w}_b^e\\\mathbf{w}_b^{e\,T}\mathbf{B}_{\theta y}^T\mathbf{B}_{yx}\mathbf{w}_b^e\\2\mathbf{w}_b^{e\,T}\mathbf{B}_{\theta x}^T\mathbf{B}_{\theta y}\mathbf{w}_b^e\end{Bmatrix}$$

$$\mathbf{k}=\begin{Bmatrix}-\frac{\partial^2\mathbf{N}_b}{\partial x^2}\mathbf{w}_b^e\\-\frac{\partial^2\mathbf{N}_b}{\partial y^2}\mathbf{w}_b^e\\-2\frac{\partial^2\mathbf{N}_b}{\partial x\partial x}\mathbf{w}_b^e\end{Bmatrix}=\begin{Bmatrix}\mathbf{B}_{kx}\\\mathbf{B}_{ky}\\\mathbf{B}_{kxy}\end{Bmatrix}=\mathbf{B}_k\mathbf{w}_b^e \quad (23)$$

and the virtual membrane strains and curvature are expressed as follows:

$$\delta\varepsilon_m=\mathbf{B}_m\delta\mathbf{w}_m^e$$

$$\delta\varepsilon_\theta=\begin{Bmatrix}\mathbf{w}_b^{e\,T}\mathbf{B}_{\theta x}^T\mathbf{B}_{\theta x}\mathbf{w}_b^e\\\mathbf{w}_b^{e\,T}\mathbf{B}_{\theta y}^T\mathbf{B}_{\theta y}\delta\mathbf{w}_b^e\\\mathbf{w}_b^{e\,T}\mathbf{B}_{\theta x}^T\mathbf{B}_{\theta y}\delta\mathbf{w}_b^e+\mathbf{w}_b^{e\,T}\mathbf{B}_{\theta y}^T\mathbf{B}_{\theta x}\delta\mathbf{w}_b^e\end{Bmatrix} \quad (24)$$

$$\delta\mathbf{k}=\mathbf{B}_k\delta\mathbf{w}_b^e$$

The electrical displacement, D_3, is the generated charge per area, A_p, of a piezoelectric material. It is assumed that D_3 is constant along the thickness direction.

$$D_3=\frac{Q}{A_p} \quad (25)$$

By using Eqs. (22) ~ (25), the element matrices are obtained and matrices which relates to electric charge can be written as follows:

$$-\int_V\delta\varepsilon_m^T\mathbf{h}^TD_3dV=\delta\mathbf{w}_m^{e\,T}\mathbf{H}_{mq}Q \quad (26)$$

$$-\int_V\delta\varepsilon_\theta^T\mathbf{h}^TD_3dV=\delta\mathbf{w}_b^{e\,T}\mathbf{H}_{1bq}^eQ+\delta\mathbf{w}_b^{e\,T}\mathbf{K}_{1bbq}^e\mathbf{w}_b^e \quad (27)$$

$$-\int_V z\delta\mathbf{k}^T\mathbf{h}^T D_3 dV=\delta\mathbf{w}_b^{eT}\mathbf{H}_{bq}^e Q \tag{28}$$

$$\int_V \delta D_3\frac{1}{\epsilon_{33}^S}D_3 dV=\delta Q_3\frac{1}{C_P^S}Q \tag{29}$$

$$\int_V -\delta D_3 h_{31}\varepsilon_x-\delta D_3 h_{31}\varepsilon_y dV=\delta Q^T\mathbf{H}_{qm}\mathbf{w}_m^{eT}+\delta Q^T\mathbf{H}_{qb}\mathbf{w}_b^{eT}+\delta Q^T\mathbf{H}_{1qb}^T\mathbf{w}_b^{eT} \tag{30}$$

where $\mathbf{H}$ is the coupling matrix between the electrical and mechanical motion and can be expressed as follows:

$$\mathbf{H}_{bq}^e=-\int_{V_p}z\mathbf{B}_k^T\mathbf{h}^T/A_P dV,\ \mathbf{H}_{mq}^e=-\int_{V_p}\mathbf{B}_m^T\mathbf{h}^T/A_P dV$$
$$\mathbf{H}_{1bq}^e=-\frac{1}{2}\int_{V_p}h_{31}(\mathbf{B}_{\theta x}^T\mathbf{B}_{\theta x}\mathbf{w}_b^e+\mathbf{B}_{\theta y}^T\mathbf{B}_{\theta y}\mathbf{w}_b^e)/A_P dV \tag{31}$$

$\mathbf{K1}_{bbq}^e(\mathrm{Q})$ is the stiffness matrix that depends linearly on the electrical charge and can be written as follows:

$$\mathbf{K1}_{bbq}^e(Q)=-\frac{1}{2}\int_{V_p}h_{31}(\mathbf{B}_{\theta x}^T\mathbf{B}_{\theta x}Q+\mathbf{B}_{\theta y}^T\mathbf{B}_{\theta y}Q)/A_P dV \tag{32}$$

After assembling the element matrices, we obtain the following discretized governing equations for electro-mechanically coupled structures.

$$\begin{aligned}&\mathbf{M}_b\ddot{\mathbf{W}}+\mathbf{G}\dot{\mathbf{W}}_b+[\lambda\mathbf{A}+\mathbf{K}_b+\mathbf{K}_{N\Delta T}\\&+\mathbf{K}_{1bbq}(Q)+\mathbf{K}_{1bbb}(\mathbf{W}_b)+\mathbf{K}_{1bbm}(\mathbf{W}_b)\\&+\mathbf{K}_{2b}(\mathbf{W}_b^2)]\mathbf{W}_b+[\mathbf{K}_{bm}+\mathbf{K}_{1bm}(\mathbf{W}_b)]\mathbf{W}_m\\&=\mathbf{P}_{b\Delta T}+\mathbf{H}_{bq}\mathbf{Q}+\mathbf{H}_{1bq}(\mathbf{W}_b)\end{aligned} \tag{33}$$

$$\mathbf{M}_m\ddot{\mathbf{W}}_m+[\mathbf{K}_{mb}+\mathbf{K}_{1mb}]\mathbf{W}_b+\mathbf{K}_m\mathbf{W}_m=\mathbf{P}_{m\Delta T}+\mathbf{H}_{mq}\mathbf{Q} \tag{34}$$

$$\mathbf{L}\ddot{\mathbf{Q}}+\mathbf{R}\dot{\mathbf{Q}}+\frac{1}{C_p^S}\mathbf{Q}=[\mathbf{H}_{bq}^T+\mathbf{H}_{1bq}^T(\mathbf{W}_b)]\mathbf{W}_b+\mathbf{H}_{mq}^T\mathbf{W}_m \tag{35}$$

Equations (33) and (34) describe the equilibrium equations of motion for the integrated system incorporating a piezoelectric material with force given by $\mathbf{HQ}$. The mechanical vibration of the piezoelectric material produces the electrical charge of the piezoelectric material, and this charge induces the piezoelectric force that suppresses the vibration of structure. Equation (35) represents the electric circuit which consists of L-R-C elements in series and clearly shows that the mechanical deformation generates an induced voltage $\mathbf{H}^T\mathbf{W}$ across the electrodes of the piezoelectric material. Equations (33) ((35) can be expressed in the form of block matrices.

$$\begin{bmatrix}\mathbf{M}_b&0&0\\0&\mathbf{M}_m&0\\0&0&L\end{bmatrix}\begin{Bmatrix}\ddot{\mathbf{W}}_b\\\ddot{\mathbf{W}}_m\\\ddot{Q}\end{Bmatrix}+\begin{bmatrix}\mathbf{G}&0&0\\0&0&0\\0&0&R\end{bmatrix}\begin{Bmatrix}\dot{\mathbf{W}}_b\\\dot{\mathbf{W}}_m\\\dot{Q}\end{Bmatrix}+\left(\begin{bmatrix}\lambda\mathbf{A}&0&0\\0&0&0\\0&0&0\end{bmatrix}+\begin{bmatrix}\mathbf{K}_b&\mathbf{K}_{bm}&-\mathbf{H}_{bq}\\\mathbf{K}_{mb}&\mathbf{K}_m&-\mathbf{H}_{mq}\\-\mathbf{H}_{bq}^T&-\mathbf{H}_{mq}^T&1/C_P^S\end{bmatrix}+\begin{bmatrix}\mathbf{K}_{N\Delta T}&0&0\\0&0&0\\0&0&0\end{bmatrix}+\begin{bmatrix}\mathbf{K}_{1bbq}(\mathbf{Q})&0&0\\0&0&0\\0&0&0\end{bmatrix}+\begin{bmatrix}\mathbf{K}_{1bbb}(\mathbf{W}_b)+\mathbf{K}_{1bbm}(\mathbf{W}_m)&\mathbf{K}_{1bm}(\mathbf{W}_b)&-\mathbf{H}_{1bq}(\mathbf{W}_b)\\\mathbf{K}_{1mb}(\mathbf{W}_b)&0&0\\-\mathbf{H}_{1bq}^T(\mathbf{W}_b)&0&0\end{bmatrix}+\begin{bmatrix}\mathbf{K}_{2b}(\mathbf{W}_b^2)&0&0\\0&0&0\\0&0&0\end{bmatrix}\right)\begin{Bmatrix}\mathbf{W}_b\\\mathbf{W}_m\\Q\end{Bmatrix}=\begin{Bmatrix}\mathbf{P}_{b\Delta T}\\\mathbf{P}_{m\Delta T}\\0\end{Bmatrix} \tag{36}$$

or,

$$\mathbf{M}\ddot{\mathbf{U}}+\mathbf{C}\dot{\mathbf{U}}+(\lambda\mathbf{A}+\mathbf{K}+\mathbf{K}_{N\Delta T}+\mathbf{K}_1+\mathbf{K}_2)\mathbf{U}=\mathbf{P} \tag{37}$$

where subscripts b and m indicate the bending and in-plane motion, respectively. $\mathbf{M}$, $\mathbf{G}$ and $\mathbf{K}$ are the element mass, aerodynamic damping, and linear stiffness matrices, respectively, and $\mathbf{K}_{N\Delta T}$ is the temperature induced geometric stiffness. $\mathbf{K}_1$ and $\mathbf{K}_2$ are the first-order and second-order nonlinear stiffness matrices which depend linearly and quadratically on the element displacements, respectively. $\mathbf{P}$ is the temperature induced load vector and $\mathbf{A}$ is the skew-symmetrical aerodynamic influence matrix. All the element matrices are symmetric except for $\mathbf{A}$. C_P^S is the inherent capacitance of the piezoelectric material.

Equation (36) is derived for one piezoelectric patch, and it can be easily extended to multiple piezoelectric patches. For example, in the case of two independent piezoelectric patches of Fig. 1, Eq. (36) can be rewritten as:

$$\begin{bmatrix}\mathbf{M}_b&0&0&0\\0&\mathbf{M}_m&0&0\\0&0&L_1&0\\0&0&0&L_2\end{bmatrix}\begin{Bmatrix}\ddot{\mathbf{W}}_b\\\ddot{\mathbf{W}}_m\\\ddot{Q}_1\\\ddot{Q}_2\end{Bmatrix}+\begin{bmatrix}\mathbf{G}&0&0&0\\0&0&0&0\\0&0&R_1&0\\0&0&0&R_2\end{bmatrix}\begin{Bmatrix}\dot{\mathbf{W}}_b\\\dot{\mathbf{W}}_m\\\dot{Q}_1\\\dot{Q}_2\end{Bmatrix}+\left(\begin{bmatrix}\lambda\mathbf{A}&0&0&0\\0&0&0&0\\0&0&0&0\\0&0&0&0\end{bmatrix}+\begin{bmatrix}\mathbf{K}_b&\mathbf{K}_{bm}&\mathbf{H}_{bq}^1&\mathbf{H}_{bq}^2\\\mathbf{K}_{mb}&\mathbf{K}_m&\mathbf{H}_{mq}^1&\mathbf{H}_{mq}^2\\\mathbf{H}_{qb}^1&\mathbf{H}_{qm}^1&1/C_{P,1}^S&0\\\mathbf{H}_{qb}^2&\mathbf{H}_{qm}^2&0&1/C_{P,2}^S\end{bmatrix}\right)\begin{Bmatrix}\mathbf{W}_b\\\mathbf{W}_m\\Q_1\\Q_2\end{Bmatrix}$$

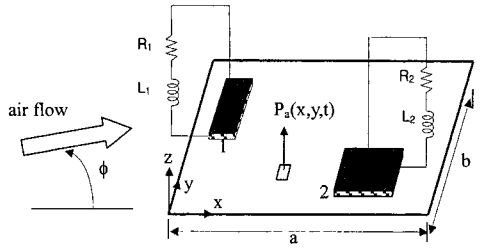

Fig. 1 Schematic diagram of a panel with two piezoelectric patches

$$
\begin{bmatrix} \mathbf{K}_{N\Delta T} & 0\ 0\ 0 \\ 0 & 0\ 0\ 0 \\ 0 & 0\ 0\ 0 \\ 0 & 0\ 0\ 0 \end{bmatrix} + \begin{bmatrix} \mathbf{K}_{1bbq}(\mathbf{Q}) & 0\ 0\ 0 \\ 0 & 0\ 0\ 0 \\ 0 & 0\ 0\ 0 \\ 0 & 0\ 0\ 0 \end{bmatrix}
$$

$$
+ \begin{bmatrix} \mathbf{K}_{1bbb}(\mathbf{W}_b)+\mathbf{K}_{1bbm}(\mathbf{W}_m) & \mathbf{K}_{1bm}(\mathbf{W}_b) & \mathbf{H}^1_{1bq}(\mathbf{W}_b) & \mathbf{H}^2_{1bq}(\mathbf{W}_b) \\ \mathbf{K}_{1mb}(\mathbf{W}_b) & 0 & 0 & 0 \\ \mathbf{H}^1_{1qm}(\mathbf{W}_b) & 0 & 0 & 0 \\ \mathbf{H}^2_{1qm}(\mathbf{W}_b) & 0 & 0 & 0 \end{bmatrix}
$$

$$
+ \left(\begin{bmatrix} \mathbf{K}_{2b}(\mathbf{W}_b^2) & 0\ 0\ 0 \\ 0 & 0\ 0\ 0 \\ 0 & 0\ 0\ 0 \\ 0 & 0\ 0\ 0 \end{bmatrix} \right) \begin{Bmatrix} \mathbf{W}_b \\ \mathbf{W}_m \\ Q_1 \\ Q_2 \end{Bmatrix} = \begin{Bmatrix} \mathbf{P}_{b\Delta T} \\ \mathbf{P}_{m\Delta T} \\ 0 \\ 0 \end{Bmatrix} \tag{38}
$$

5. Solution Procedure

In the development of a flutter suppression strategy, it is generally impractical to consider all modeled modes because of large degrees of freedom of the system involved. This section describes the methods for modal transformation. The generation of a large piezoelectric force is needed to suppress flutter effectively, and piezoceramic material(PZT) satisfies this requirement. In the design of PZT, the optimal placement of PZT is calculated to maximize the piezoelectric force, and the genetic algorithm is used as an optimization method.

5.1 Model equations

Equation (37) can be changed to the properly chosen modal coordinates by the following modal transformation.

$$\mathbf{U}=\sum_{r=1}^{m}\sum_{s=1}^{n}\eta_{rs}(t)\{\phi_{rs}\} \tag{39}$$

where η_{rs} is the modal displacement vector and $\{\phi_{rs}\}$ is the normal mode vector obtained by solving the eigenvalue problem of the form

$$\mathbf{K}\{\phi_{rs}\}=\mu\mathbf{M}\{\phi_{rs}\} \tag{40}$$

It is well known that the response of the panel flutter produces good results even though only the first six modes (m=1, 2, 3, 4, 5, 6) are considered in the airflow direction and the first mode (n=1) alone is considered in the spanwise direction (Dowell, 1966). Then, Eq. (39) becomes

$$\mathbf{U}=\sum_{r=1}^{m}\eta_r(t)\{\phi_r\}=\boldsymbol{\Phi}\boldsymbol{\eta} \tag{41}$$

Substituting Eq. (41) into Eq. (37), the system equations of motion (37) can be expressed as follows:

$$\tilde{\mathbf{M}}\boldsymbol{\eta}_{,\tau\tau}+\tilde{\mathbf{C}}\boldsymbol{\eta}_{,\tau}+(\tilde{\mathbf{K}}+\tilde{\mathbf{K}}_{\eta}+\tilde{\mathbf{K}}_{\eta\eta})\,\boldsymbol{\eta}=\tilde{\mathbf{P}} \tag{42}$$

where $\tau=\omega_0 t$ is the nondimensionalized time variable, and the modal stiffness matrices and modal thermal force vector are expressed as follows:

$$
\begin{gathered}
\tilde{\mathbf{K}}=\boldsymbol{\Phi}^T(\lambda\mathbf{A}+\mathbf{K}+\mathbf{K}_{N\Delta T})\,\boldsymbol{\Phi} \\
\tilde{\mathbf{K}}_{\eta}=\boldsymbol{\Phi}^T\mathbf{K}_1\boldsymbol{\Phi},\ \tilde{\mathbf{K}}_{\eta\eta}=\boldsymbol{\Phi}^T\mathbf{K}_2\boldsymbol{\Phi} \\
\tilde{\mathbf{P}}=\boldsymbol{\Phi}^T\mathbf{P}
\end{gathered} \tag{43}
$$

The reduced nonlinear modal equation of motion, Eq. (42), can be solved using time numerical integration scheme such as the Newmark-β method.

5.2 Optiamal shape and locations of piezoelectric materials

As the piezoelectric force $\mathbf{H}\mathbf{Q}$ is increased, the damping effect induced by the piezoelectric patch is increased. Additionally, a larger induced voltage $\mathbf{H}^T\mathbf{W}$ increases the dissipation of the electrical energy through the resistor in the electric circuit. Moreover, the damping effect can be effectively augmented if the electro-mechanical coupling matrix $\mathbf{H}$ is designed to increase the piezoelectric force corresponding to the modes that are to be suppressed. Note that the electro-mechanical coupling matrix, $\mathbf{H}$, depends on the locations of the piezoelectric patch as well as the piezoelectric material property h_{31}. Therefore, it is desirable to place the piezoelectric patch at the location that maximizes the modal piezoelectric force. Based on this observation, the optimal shape and location of the piezoceramic patch can

be determined through optimization by the genetic algorithm(Tang et al., 1999), with the number and sizes of the piezoceramic patches given as inputs. When an element is covered with piezoceramic patches, that element is turned on; when an element is not covered, it is turned off. The performance index used in the optimization process can be defined by

$$J=Min(|\phi^T\mathbf{H}|)_c \tag{44}$$

where $\phi^T\mathbf{H}$ is associated with the modal piezoelectric force per unit charge, and the subscript c is the mode to be suppressed. ϕ is a column matrix composed of the eigenvectors of the modes to be suppressed and it is assumed that the plate is perfectly bonded to the plate.

$$\begin{bmatrix}\mathbf{K}_b & \mathbf{K}_{bm}\\ \mathbf{K}_{mb} & \mathbf{K}_m\end{bmatrix}\phi=\bar{\lambda}\begin{bmatrix}\mathbf{M}_b & 0\\ 0 & \mathbf{M}_m\end{bmatrix}\phi \tag{45}$$

The maximization of J gives the optimal design.

After the optimal shape and locations of the piezoelectric patch are determined, the optimum magnitudes of the resistance and inductance must be determined, and those values can be obtained by the pole placement method (Hagood and Flotow, 1991).

6. Numerical Results

Passive suppression of nonlinear panel flutter is numerically tested. The six-coupled nonlinear equations of the modes denoted by the modal indices, $(m, n)=(1, 1)$ and $(2, 1)$-$(6, 1)$, are integrated by using the Newmark-β method and the responses of the panel motion are calculated at a location with coordinates x=0.75a and y=0.5b. For the analyses, a simply supported [45°/-45°/90°/0°]$_s$ square graphite/epoxy composite plate is modeled. The material properties of the graphite/epoxy composite and piezoelectric materials are summarized in Table 1. The dimensions of the composite plate are 0.3×0.3×0.001m. The piezoelectric patch is bonded at the bottom side of the panel to avoid obstructing the airflow, and the piezoelectric layer thickness is assumed to be 0.0005m.

The temperature distribution in all cases is assumed to be $\Delta T=T_o\sin(\pi x/a)\sin(\pi y/b)$, and the aerodynamic damping coefficient is assumed to be $\mu/M_\infty=0.01$.

Table 1 Material properties

Property	Gr/Epoxy	PZT (PSI-5A-S4-ENH)
Elastic property		
E_1(GPa)	155	66
E_2(GPa)	8.07	66
G_{12}(GPa)	4.55	25.38
ν_{12}	0.22	0.3
Thermal expansion(10^{-6}/℃)		
a_1	−0.07	4
a_2	30.1	4
Piezoelectric coefficient(10^{-12}m/V)		
d_{31}	0	−190
Electric permittivity		
$\in_{33}^T/\in_o$	0	1880
($\in_o$ =8.85 ×10^{-12} farads/m)		
Mass density(kg/m^3)	1550	7800

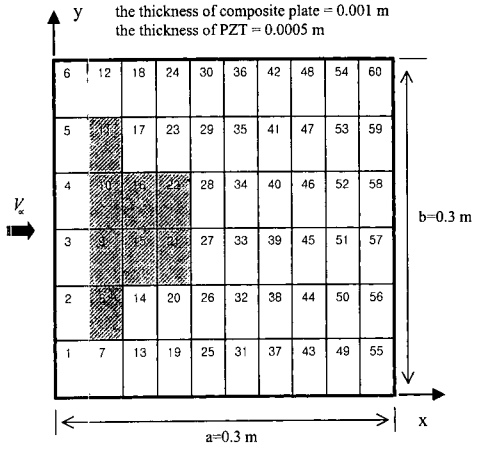

Fig. 2 The shape and the locations of piezoceramic patches

The critical buckling temperature of the panel is calculated to be 16.6℃ for the panel as shown in Fig. 2.

In Fig. 3, the modal frequency and damping ratio of the plate are calculated as a function of inductance at a fixed resistance (R=3899Ohm). It is found that the optimal inductance, which produces the maximum damping ratio, is 25

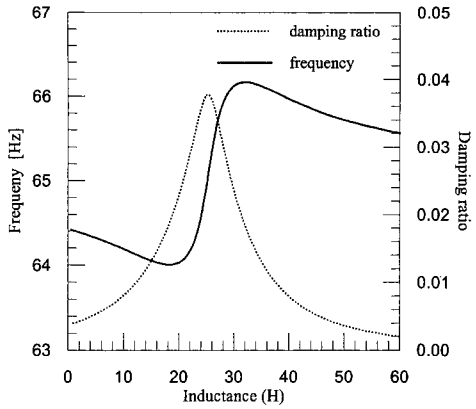

Fig. 3 Effects of inductance on the modal frequency and damping ratio for first flutter mode(1, 1) (R=3899Ω)

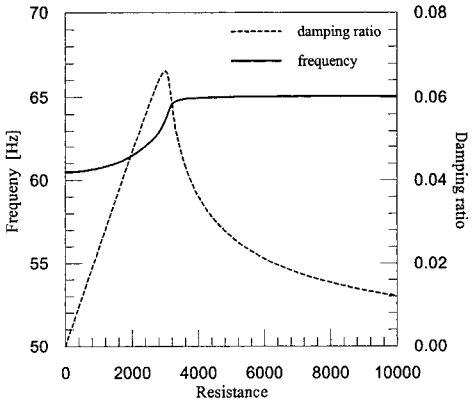

Fig. 4 Effects of inductance on the modal frequency and damping ratio for first flutter mode(1, 1) (L=25H)

Henry and that the maximum shifts of the modal frequencies occur near the point of the maximum damping ratio.

In Fig. 4, the modal frequency and damping ratio of the flutter mode (1, 1) are calculated as a function of the resistance at fixed optimal inductance value (25 Henry) given in Fig. 3. It is observed that the optimal resistance, which produces the maximum damping ratio, is 2800 Ohm. It is also observed that the maximum shift of the modal frequency occurs near the point of maximum damping ratio as in the previous case.

A larger portion of the electrical energy is dissipated in the resistor during a vibration cycle

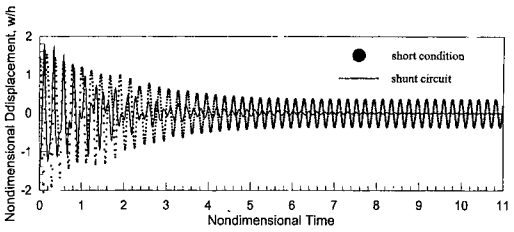

Fig. 5 Time history of panel motion at short circuit condition and shunted circuit of L=25H, R=2.8KΩ($\Delta T/\Delta T_{cr}$=0, λ=290)

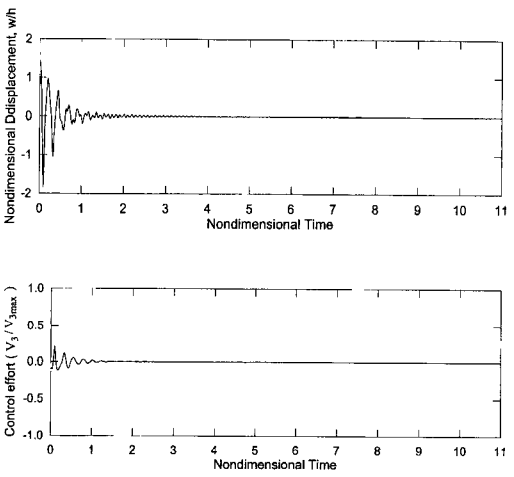

Figure 6. Time history of panel motion for active control case ($\Delta T/\Delta T_{cr}$=0, λ=290).

Fig. 6 Time history of panel motion for active control case($\Delta T/\Delta T_{cr}$=0, λ=290)

when the optimal inductance and resistance are used.

Figure 5 shows that the panel motion at the short circuit condition becomes a limit-cycle vibration under the dynamic pressure λ=290 without a thermal load and that the limit-cycle can be suppressed completely with optimal resistance(2.8KΩ) and inductance(25H). Figure 6 shows the time history of the plate deflection and the control voltage for the active control case. The plate deflection is shown to be suppressed within several cycles after the controllers are activated. As shown in Figs. 5 and 6, the performance of the passive damping method is not superior to that of the active control case(Zhou et al., 1995).

Figure 7 shows that the panel motion at the short circuit condition becomes a limit-cycle in

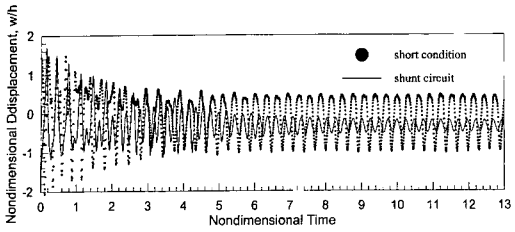

Fig. 7 Time history of panel motion at short circuit condition and shunted circuit of L=25H, R=2.8KΩ ($\Delta T/\Delta T_{cr}=1.6$, $\lambda=180$)

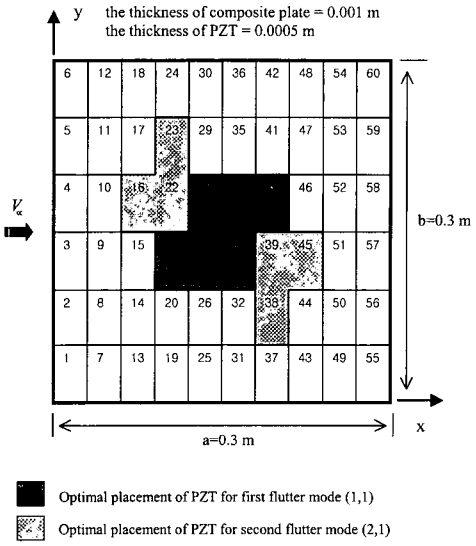

Fig. 8 Optimal shape and locations of piezoceramic patches

the case of the dynamic pressure $\lambda=180$ and temperature load of $\Delta T/\Delta T_{cr}=1.6$. The motion of panel with shunted circuit changes into a limit-cycle, and the amplitude of the limit-cycle is reduced to just one-third of the original amplitude due to increased passive damping as shown in Fig. 7.

Next, we design the suppression system with two independent sets of piezoceramic patches for multimodal suppression. To obtain the optimal shape and locations of the piezoceramic patches, the genetic algorithm is implemented in the computer program we developed. During the design of the piezoceramic patches, it is assumed that the size and number of the piezoceramic patches are constant, and the number of piezoceramic patches is six for each mode in Fig. 8. The darker area is

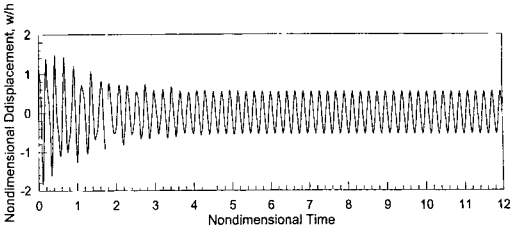

Fig. 9 Time history of panel motion at short circuit condition ($\Delta T/\Delta T_{cr}=0$, $\lambda=360$)

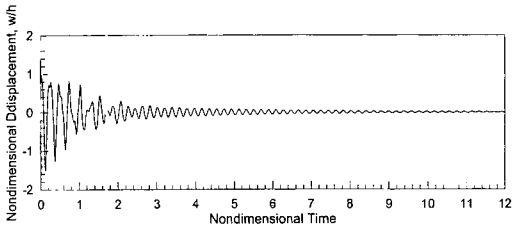

Fig. 10 Time history of panel motion with shunted circuits of $L_1=40H$, $L_2=7.3H$, $R_1=6618\Omega$, $R_2=3094\Omega$ ($\Delta T/\Delta T_{cr}=0$, $\lambda=360$)

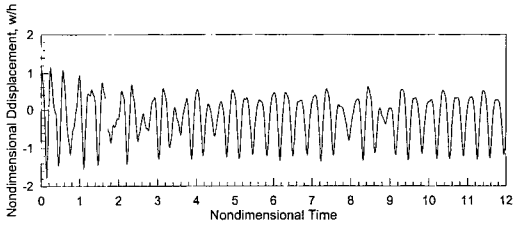

Fig. 11 Time history of panel motion at short circuit condition ($\Delta T/\Delta T_{cr}=3$, $\lambda=150$)

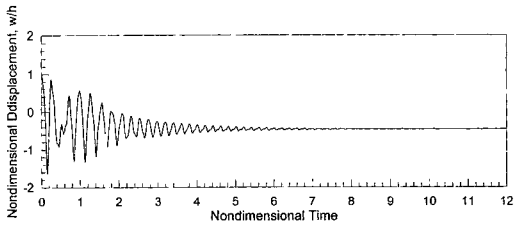

Fig. 12 Time history of panel motion with shunted circuits of $L_1=40H$, $L_2=7.3H$, $R_1=6618\Omega$, $R_2=3094\Omega$ ($\Delta T/\Delta T_{cr}=3$, $\lambda=150$)

the optimal patch shape for the first flutter mode (1, 1), and the lighter area is the optimal patch for the second flutter mode(2,1). For optimization using the genetic algorithm, the population is set at 600, the crossover probability

at 0.9, and the mutation probability at 0.03. Each independent piezoelectric element is connected with a L-R series circuit.

As shown in Fig. 9, the panel vibrates as a limit-cycle motion when the short circuit condition is under $\lambda=360$ and there is no thermal load. The limit-cycle oscillation can be suppressed completely by two-resonant shunt circuits with $L_1=40H$, $L_2=7.3H$, $R_1=6618\Omega$, $R_2=3094\Omega$ as shown in Fig. 10.

The chaotic motion of the panel at moderate temperature conditions can be completely suppressed by two-resonant shunt circuits as shown in Figs. 11 and 12.

7. Concluding Remarks

A passive suppression scheme for nonlinear panel flutter was proposed by using one L-R series shunt circuit and two independent L-R shunt circuits. The equations of motion of the plate including the piezoelectrics and shunted circuits are discretized by the finite element method. An optimal shape and location that maximizes the piezoelectric force of the piezoceramic was determined by using the genetic algorithms. By applying the Newmark-β method, the effects of passive suppression for composite panel flutter were investigated in the time domain. It was shown that the performance of two independent L-R shunt circuits is superior to that of single shunt circuit. This study clearly demonstrates that the passive control using the piezoelectric shunt circuit is effective in panel flutter suppression. The active control system has the advantage of being adaptable to a variety of system changes through feedback or feedforward actions and also has a higher performance in comparison with the passive system. However, application of the active control method practical flutter suppression means that a large amount of power is required to operate actuators. Also, the active system has the spillover problem and is sensitive to system uncertainties. Although the performance of the passive damping is not superior to that of the active control method, it is noted that the passive damping scheme is always robust and there is no need for additional hardware such as sensors and actuators, and there is also no need for control instruments. Therefore, the suppression scheme based on passive damping can be preferable in practice for suppression of panel flutter.

Acknowledgements

This study was supported by the Ministry of Science and Technology through National Research Laboratory Program(00-N-NL-01-C-026).

References

Chia C. Y., 1980, "Nonlinear Analysis of Plates," McGraw-Hill, pp. 1~21.

Dowell, E. H., 1966, "Nonlinear Oscillations of a Fluttering Plate," *AIAA journal* Vol 4, No. 7, pp. 1267~1275.

Goldberg, D. E., 1989, *Genetic Algorithms in Search, Optimization & Machine Learning*, Addison-Wesley.

Hagood, N. W., and Flotow, A. V., 1991, "Damping of Structural Vibrations with Piezoelectric Materials and Passive Electrical Networks," *Journal of Sound and Vibration*, Vol. 146, No. 2, pp. 243~268.

Hollkamp, J. J., 1994, "Multimodal Passive Vibration Suppression with Piezoelectric Materials and Resonant Shunts," *Journal of intelligent Material Systems and Structures*, Vol. 5, No. 1, pp. 49~57.

Hollkamp, J. J and Gorden, R. W., 1995, "An Experimental Comparison of Piezoelectric and Constrained Layer Damping," *Proceedings of SPIE Smart Structures and Materials Conference*, Vol. 2445, pp. 123~133.

Kim, S. J., Han, C. H., and Yun., C. Y. 1999, "Improvement of aeroelastic stability of hingeless helicopter rotor blade by passive piezoelectric damping," *Proceedings of SPIE Smart Structures and Materials Conference*, Vol. 1991, pp. 1552~1561.

Lee, J. K., Cheong, C. C., and Kim J. H., 1999, "Piezoelectric Smart Structures for Noise Reduc-

tion in a Cabin," *KSME International Journal*, Vol. 13, No. 6, pp. 451~458.

Nam, C. H., and Kim, J. S., 1996, "H$^{\infty}$ Control for Flutter Suppression of a Laminated Plate with Self-Sensing Actuators," *KSME International Journal*, Vol. 10, No. 2, pp. 169~179.

Scott, R. C., and Weisshaar, T. A., 1994, "Controlling Panel Flutter Using Adaptive Materials," *Journal of aircraft*, Vol. 31, No. 1, pp. 213~222.

Tang, J., Wang, K. W., and Philen, M., 1999, "Sliding Mode Control of Structural Vibrations via Active-Passive Hybrid Piezoelectric Network," *Proceedings of SPIE Smart Structures and Materials Conference* (Newport Beach, California), Vol. 3668, pp. 543~553.

Zhou, R. C., LAI, Z., Xue, D. Y., Hauang, J. -K., and Mei, C., 1995, "Suppression of Nonlinear Panel Flutter with Piezoelectric actuators Using Finite Element," *AIAA Journal*, Vol. 33, No. 6, pp. 1098~1105.

Appendix

A.1 Derivation of Piezoelectric Constant h_{31}

The two piezoelectric constitutive equations (g-form) necessary to find the piezoelectric constant h_{31} are

$$\boldsymbol{\varepsilon}=\boldsymbol{s}^{D}\boldsymbol{\sigma}+\boldsymbol{g}^{T}\boldsymbol{D} \tag{A1}$$

$$\boldsymbol{E}=-\boldsymbol{g}\boldsymbol{\sigma}+\boldsymbol{\beta}^{t}\boldsymbol{D} \tag{A2}$$

The derivation of the constitutive equations of a piezoelectric material in this study is based on the following assumptions: (1) The 3-direction (w-direction) is associated with the direction of poling and the piezoelectric material (PZT) is approximately isotropic in the other two inplane directions, and (2) the only nonzero component of the electric field and displacement is E_3 and D_3, respectively.

Applying assumptions (1) and (2), Eqs. (A1) and (A2) can be written by

$$\begin{Bmatrix}\varepsilon_x\\ \varepsilon_y\\ \gamma_{xy}\end{Bmatrix}=\begin{bmatrix}s_{11} & s_{12} & 0\\ s_{12} & s_{11} & 0\\ 0 & 0 & 2(s_{11}-s_{12})\end{bmatrix}^{D}\begin{Bmatrix}\sigma_x\\ \sigma_y\\ \tau_{xy}\end{Bmatrix}_{p}+\begin{Bmatrix}g_{31}\\ g_{31}\\ 0\end{Bmatrix}D_3 \tag{A3}$$

$$E_3=-\begin{bmatrix}g_{31} & g_{31} & 0\end{bmatrix}\begin{Bmatrix}\sigma_x\\ \sigma_y\\ \tau_{xy}\end{Bmatrix}+\beta_{33}^{t}D_3 \tag{A4}$$

where

$$s_{11}=\frac{1}{E},\ s_{11}=-\frac{\nu}{E}$$

Adding Eqs. (A3) and (A4) yields

$$\sigma_x+\sigma_y=\frac{(\varepsilon_x+\varepsilon_y)-2g_{31}D_3}{s_{11}^{D}+s_{12}^{D}} \tag{A5}$$

Substuting Eq. (A5) into Eq. (A4) yields

$$\begin{aligned}E_3&=-\begin{bmatrix}\frac{g_{31}}{s_{11}^{D}+s_{12}^{D}} & \frac{g_{31}}{s_{11}^{D}+s_{12}^{D}} & 0\end{bmatrix}\begin{Bmatrix}\varepsilon_x\\ \varepsilon_y\\ \gamma_{xy}\end{Bmatrix}+\left[\frac{2g_{31}^{2}}{s_{11}^{D}+s_{12}^{D}}+\beta_{33}^{t}\right]D_3\\ &=-\begin{bmatrix}g_{31}(c_{11}^{D}+c_{12}^{D}) & g_{31}(c_{11}^{D}+c_{12}^{D}) & 0\end{bmatrix}\begin{Bmatrix}\varepsilon_x\\ \varepsilon_y\\ \gamma_{xy}\end{Bmatrix}\\ &\quad+\left[2g_{31}^{2}(c_{11}^{D}+c_{12}^{D})+\beta_{33}^{t}\right]D_3 \qquad (A6)\\ &=-\begin{bmatrix}h_{31} & h_{31} & 0\end{bmatrix}\begin{Bmatrix}\varepsilon_x\\ \varepsilon_y\\ \gamma_{xy}\end{Bmatrix}+\beta_{33}^{s}D_3 \text{(from } Eq.(2))\end{aligned}$$

Therefore, the piezoelectric constant h_{31} can be written as

$$h_{31}=g_{31}(c_{11}^{D}+c_{12}^{D}) \tag{A7}$$